PCCP

PAPER

View Article Online
View Journal

Cite this: DOI: 10.1039/d6cp00367b

The effect of localisation imprecision on quantification of the directionality of motion for single particle tracking applications

Paula Melero Martinez and Christoffer Åberg *

The tracking of single molecules, nanoparticles, or even intracellular vesicles using microscopy is a common approach across different fields of science. In such applications, invariably the particle can only be localised with finite precision, leading to an associated error in all observables of the motion. While the effect of localisation imprecision in, for example, the mean square displacement is well understood, the situation is less clear when it comes to assessments of the directionality of motion. Here we study the role played by localisation imprecision for several different measures of the directionality of motion. We study stationary particles and particles moving by Brownian motion both experimentally and theoretically. We show that localisation imprecision alone gives rise to a substantial degree of anti-directional motion. Comparison between theory and experiments shows excellent agreement, implying a good understanding and control of the effect. Overall, our results can be used to predict the role played by localisation imprecision when studying the directionality of motion using single particle tracking and suggest caution when interpreting such data.

Received 31st January 2026,
Accepted 27th May 2026

DOI: 10.1039/d6cp00367b

rsc.li/pccp

Groningen Research Institute of Pharmacy, University of Groningen, A. Deusinglaan 1, 9713 AV Groningen, The Netherlands. E-mail: christoffer.aberg@rug.nl

Christoffer Åberg

Christoffer Åberg has a background in theoretical physics, holding an MSc in physics from Lund University, Sweden (2005). He went on to do a PhD in physical chemistry, also at Lund University (2009), working on theoretical studies of diffusion in colloidal systems. Subsequently, he moved towards biology, applying his physics/colloid science background to how nano-sized objects interact with cells, at University College Dublin, Ireland. Since 2014 he has been at the University of Groningen, The Netherlands and is currently an associate professor at the Groningen Research Institute of Pharmacy. His main research interests revolve around intracellular motion and how it relates to nanoparticle distribution in cells.

Introduction

In complex systems such as polymer networks,[1] reconstituted actin networks,[2] bacteria,[3] amoeba,[4] or human cells,[5] the motion of embedded probe particles can help elucidate the structure and dynamics of the system. In living cells, the motion is additionally not only useful as a tool but also of importance itself, as many biological processes depend upon a molecule or vesicle travelling from one place to another. A frequent method to follow such motions is to observe the particles with microscopy and simply track each individual particle for as long as possible.[6,7] Indeed, this practice dates back already to Perrin and Nordlund's investigations of Brownian motion at the beginning of the last century,[8] but has been much invigorated by modern microscopy methods and thus expanded to a broad range of different studied systems.[9–17]

A fundamental tenet of such studies is that there is a limit to how well a particle can be localised. In classical microscopy methods, this limit is ultimately set by diffraction,[18] though it can be much improved by collecting more and more photons.[19] Modern super-resolution methods[20] can push the localisation imprecision (further) down compared to the diffraction limit but naturally there nevertheless remains a finite limit.

Clearly the finite precision with which one can localise a particle has to be taken into account when assessing its motion. When it comes to the *extent* of the motion, the effect is fairly well-known. For example, how localisation imprecision affects

the mean square particle displacement, a very typical observable for how far a particle moves, has been well-studied.[21–24] However, the situation is less investigated when it comes to the *directionality* of the motion. Previous work has shown that immobilised particles, whose observed motion presumably only stems from localisation imprecision, exhibit a non-uniform distribution of the angle corresponding to the change in direction,[25,26] but not demonstrated the origin. Furthermore, the effect of localisation imprecision on the directionality of motion has been discussed in the context of a generalised Langevin equation model[27] as well as for Brownian motion,[28] but only at an average level.

Here we demonstrate in detail the effect of particle localisation imprecision on various measures of the directionality of their motion. We start by considering stationary particles, whose lack of motion may suggest trivial outcomes, but where we actually observe strong anti-directional motion stemming solely from localisation imprecision. We study this in detail, both experimentally and theoretically and for a range of observables: the average angle, the average cosine of the angle, the full distribution of the angle, the average scalar product between displacement vectors (related to the velocity autocorrelation function), and the full distribution of the scalar product between displacement vectors. In all cases we find excellent agreement between experiments and theory. We then generalise the whole theoretical description to particles moving by Brownian motion, and confirm the outcomes using simulations. Overall, we demonstrate the surprisingly large effect of localisation imprecision on quantification of the directionality of motion, suggesting that this needs to be carefully considered when interpreting experimental results.

Experimental

Experimental procedure

A dispersion was prepared of 200 nm diameter yellow/green carboxylated polystyrene particles (Life Technologies) in Dulbecco's Modified Eagle Medium (DMEM; Gibco) supplemented with 10% foetal bovine serum (ThermoFisher Scientific) at a concentration of 50 μg ml^{-1}. 1 ml of the particle dispersion was added to a Petri dish with a glass-bottom microwell (MatTek, Ashland, MA, USA) and left for 20 min for the particles to adhere to the glass surface. Subsequently, the particle dispersion was discarded, the Petri dish was washed with 1 ml Dulbecco's Phosphate-Buffered Saline without calcium and magnesium (DPBS; Gibco) and 1 ml of medium was added.

The particles were imaged at 37 °C and 5% CO_2 with a Nikon Eclipse Ti2-E inverted microscope using a 60× oil immersion objective (Plan Apo NA = 1.42; Nikon) and a 1.518 refractive index oil (Nikon, type F). The Petri dish was left on the microscopy stage for 10 min prior to commencing image acquisition in order to minimize drift, both in the acquisition plane and along the optical axis. The particles were imaged with a 470 nm LED light, using a 446–486 nm excitation filter and a 500–550 emission filter at 2% power (arbitrary units) and with 20 ms exposure time. A widefield fluorescence time series of a region of interest of 512 × 512 pixels (see Fig. 1a below) was acquired for a total duration of 50 s at a 50 ms frame rate (resulting in 1001 frames).

Particle tracking

The time series was analysed using ImageJ[29]/Fiji[30] (version 2.16.0), an open-source package for image analysis. Particles were excluded from analysis by visual inspection as follows: some particles appeared larger, that is, exhibited stronger fluorescence, than the average and were excluded because they could be agglomerates; some particles were visibly shaking during the acquisition and were excluded because they were likely not strongly adsorbed to the glass surface; and some particles were transiently obscured when a particle still in dispersion diffused over them. A mask was created to exclude these particles.

The particles were tracked with TrackMate (version 7.14.0),[31] an ImageJ plugin. The position of the particles was localized in

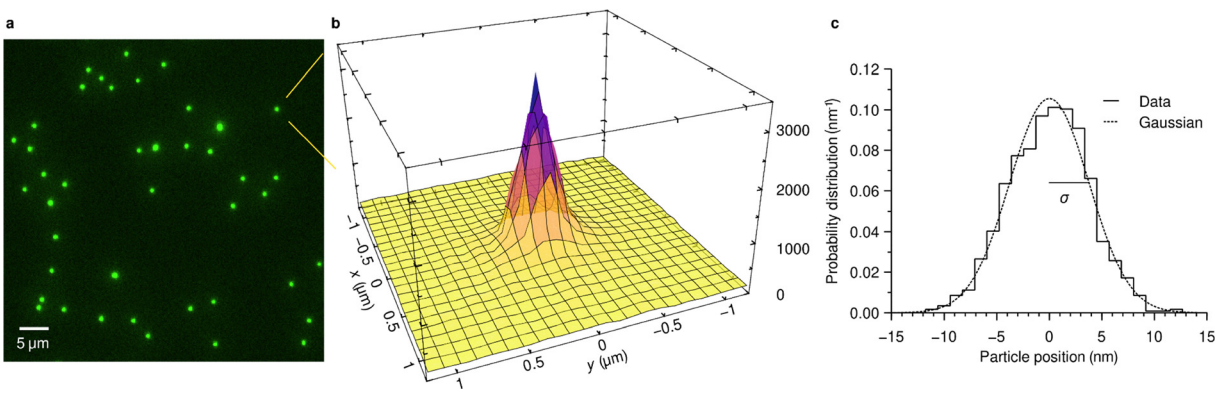

Fig. 1 Localisation imprecision of particles adhering to glass. (a) Widefield fluorescence image of 200 nm diameter particles adhering to glass. (b) Fluorescence intensity distribution of the particle indicated in panel a. The size of the grid is given by the size of a pixel. (c) The x coordinate of the same particle extracted from 1001 images. The extracted x coordinate varies somewhat image-by-image so we find a distribution of values. (Solid line) Distribution of the x coordinate after subtracting its mean. (Dotted line) Gaussian corresponding to the maximum likelihood estimated scale parameter [*i.e.*, the σ in $(2\pi\sigma^2)^{-\frac{1}{2}} \exp(-0.5x^2/\sigma^2)$] of 3.8 nm.

every frame using the Difference of Gaussians detector with sub-pixel localization enabled and no median filter used. The background threshold was set to 68 and the object diameter to 0.75 μm. Detected objects in different frames were linked to form trajectories using the Simple Linear Assignment Problem tracking algorithm. The linking and gap closing max distance were both set to 1 μm and the max frame gap was set to 1 frame. All trajectories were manually reviewed.

Trajectory analysis

Drift removal. Prior to analysis, the drift was estimated by calculating the displacement as a function of time and averaging this over all particles. This was subtracted from all particle trajectories.

Localisation imprecision. The localisation imprecision of a given particle/trajectory was calculated as follows: The mean position was averaged over the whole trajectory and subtracted from all positions. Subsequently, the scale parameter of a zero mean Gaussian maximum likelihood estimate to these fluctuations in position was calculated. In one dimension this was done using SciPy (version 1.9.1)[32] corresponding to the estimator

$$\hat{\sigma} = \sqrt{\frac{1}{n}\sum_{i=1}^{n} x_i^2}$$

while in two dimensions this was done using the estimator

$$\hat{\sigma} = \sqrt{\frac{1}{2n}\sum_{i=1}^{n} (x_i^2 + y_i^2)}.$$

The scale parameter was used as localisation imprecision, as described below.

Directionality quantification. The cosine of the angle between displacements along a trajectory was calculated from the scalar product of the displacements vectors [eqn (1) below]; the scalar product between displacement vectors itself was also considered [eqn (3) below]. For results corresponding to single trajectories the results were pooled together over all displacements separated by the same amount of time (lag time); for results of all trajectories the results were subsequently pooled together over all trajectories (ensemble and lag time).

Simulations of Brownian motion

Particles moving by Brownian motion with a diffusion coefficient, D, in two-dimensions were simulated as follows: 10^6 independently moving particles were initiated at the origin. A Gaussian-distributed localisation imprecision with mean 0 and scale parameter σ was added to the particles' positions to give observed initial positions. The time interval between subsequent observations was set to 1 and discretized into 1000 substeps of length $dt = 10^{-3}$. For each particle, a substep size was taken from a Gaussian distribution with mean 0 and scale parameter $\sqrt{(2Ddt)}$ for both the x and y directions. The step sizes were added to the real (not observed) coordinates of the particles. This was repeated 999 more times, after which a new observed position of the particles was recorded by adding localisation imprecision as before. This overall procedure was repeated one more time to give, in total, 3 observed positions (including the observed initial position). The observed positions were subsequently treated in the same way as the experimental data.

Results and discussion

Initial considerations

To study the effect of localisation imprecision on directionality quantification we started by investigating particles adsorbed to glass. As a model system we used 200 nm diameter fluorescent polystyrene particles and observed them using fluorescence microscopy at 37 °C and 5% CO_2 (similar to live-cell experiments). Fig. 1a shows an example image of the particles adhering to glass. The size of a pixel is here 108 nm but since such images are diffraction-limited the extent of a pixel is not what sets the resolution of the image; rather the resolution is roughly given by $\sim\lambda/2$, where λ is the wavelength of the light.[18,19] In this case λ = 470 nm and the resolution is thus $\sim$230 nm. Indeed, the particles in the image do not appear as well-localised images of 200 nm-sized objects, but rather the observed fluorescence emanating from a particle is spread out over a larger area (Fig. 1b). Super resolution approaches can ameliorate this,[20] but requires more specialised equipment and often implies other limits (*e.g.*, a slower rate of acquisition).

The distribution of fluorescence stemming from a particle is well-approximated by a Gaussian (Fig. 1b), which implies that one can localise the particle by fitting a Gaussian to the fluorescence distribution to find its centre. This procedure is used in many particle tracking software packages, including the ImageJ[29]/Fiji[30] plugin TrackMate[31] used here, and typically results in a better localisation than what both the resolution limit and the size of a pixel would suggest. As an illustration consider the particle whose fluorescence distribution is shown in Fig. 1b. This particle was imaged by microscopy 1001 times in rapid succession and its coordinates extracted from each of these images after drift correction (see Experimental section). The distribution of, say, the x coordinate is well-described by another Gaussian (Fig. 1c). The scale parameter in this case is σ = 3.8 nm which thus gives a measure of how well we are able to localise this particular particle. Importantly, we are able to localise the example particle in Fig. 1 (σ = 3.8 nm) much better than what both the resolution limit ($\sim$230 nm) and the size of a pixel (108 nm) would suggest.

In the following, we will use the maximum likelihood estimate of the scale parameter σ of a two-dimensional Gaussian (as opposed to the one-dimensional version used for illustrative purposes in Fig. 1c) and refer to it as the particle localisation imprecision. We should note that in general there are situations when a Gaussian is not a good approximation, for example, if the background noise is comparable in strength to the signal, the microscopy stage is drifting, or the particle is moving.

Naturally, the finite localisation imprecision will have to be taken into account when assessing any observable of motion

investigated using microscopy. For example, for diffusive motion it is well-known that localisation imprecision changes the mean square displacement in terms of an additive offset.[21–23,33] Indeed, experimental studies (*e.g.*, of mRNA particles in *Saccharomyces cerevisiae*[34] or of the transmembrane protein CD44 in fibroblast cells[35]) routinely consider a non-zero (extrapolated) intercept of a mean square displacement curve to be due to finite localisation imprecision.[36] The effect of localisation imprecision on the mean square displacement of fractional Brownian motion has also been considered.[24] It has even been demonstrated how the observed type of motion can change from diffusive to subdiffusive depending upon the extent of localisation imprecision.[22] Naturally localisation imprecision also influences the displacement distribution and can in extreme cases result in equidistant peaks if subpixel localisation is not used.[17] In contrast to these measures of the *extent* of motion, the effect of localisation imprecision on assessments of the *directionality* of motion is less investigated. This is the subject to which we now turn.

Directionality of motion

We start by defining how we will characterise the directionality of motion. Let us consider the position of a particle $\mathbf{r}(t)$ defined as a function of time t. When assessed using microscopy, the trajectory is only sampled at discrete times (Fig. 2a dots), where those times are typically chosen equidistant from each other (or at least approximately so, to the degree allowed by the experimental set-up). Between any two times, we can form a displacement vector which will then tell in which direction the particle moved (nett) between those two times (Fig. 2a arrows). Often these directions are not by themselves interesting, as many systems considered are isotropic at some scale; however, the angle *between* displacements (Fig. 2a angle θ) is often of interest as a means of characterising the motion. This angle can report upon the degree to which a particle keeps moving in the same direction, whether the particle reverses direction, and the timescales for such processes.[27,28,37–40]

We thus consider the angle θ between displacements defined by

$$\cos\theta = \frac{\Big(\mathbf{r}(t+\Delta\tau)-\mathbf{r}(t)\Big)\cdot\Big(\mathbf{r}(t+\tau+\Delta\tau)-\mathbf{r}(t+\tau)\Big)}{\Big|\mathbf{r}(t+\Delta\tau)-\mathbf{r}(t)\Big|\Big|\mathbf{r}(t+\tau+\Delta\tau)-\mathbf{r}(t+\tau)\Big|}. \quad (1)$$

Note that compared to previous literature,[27,28,37] we have generalised the definition somewhat by using two timescales: the first one $\Delta\tau$ is used to define the displacement vector and hence the timescale we define the direction over (*cf.* Fig. 2a and b where $\Delta\tau$ is twice as large in panel b as in a). The other timescale τ is used for the timescale over which we are interested in investigating if the direction is kept. Thus, we consider the angle both between successive displacements (Fig. 2a; *e.g.*, displacement between $t = 0$ and $t = t_1$, and displacement between $t = t_1$ and $t = t_2$) as well as displacements separated in time from each other (Fig. 2a; *e.g.*, displacement between $t = 0$ and $t = t_1$, and displacement between $t = t_2$ and $t = t_3$).

We also note that the numerator of eqn (1) is closely related to what is sometimes termed the velocity autocorrelation function defined by[8]

$$C_{v;\Delta\tau}(\tau) = \frac{1}{\Delta\tau^2}\Big\langle\Big(\mathbf{r}(t+\Delta\tau)-\mathbf{r}(t)\Big)\cdot\Big(\mathbf{r}(t+\tau+\Delta\tau)-\mathbf{r}(t+\tau)\Big)\Big\rangle \quad (2)$$

something we will also consider.

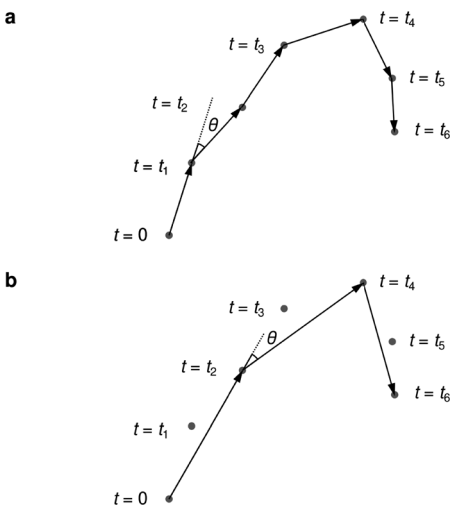

Fig. 2 Definition of directionality. (a) The trajectory of a particle assessed using microscopy. The (approximate) location of the particle (dots) is sampled at discrete times $t = t_1, t_2,$ *etc.* Between each pair of such sampled locations we can form a displacement vector (arrows) and define the change in direction (angle θ) between displacements. (b) It is also possible to follow the change in direction (angle θ) over longer time-intervals, in this case between every other frame.

Directionality of stationary particles – experimental observations

We now assess the directionality of particles adsorbed to glass (*cf.* Fig. 1). Terms like displacements and directionality are then misnomers, as the particles are stationary and any displacement and directionality of the motion actually stem from localisation imprecision. However, as will transpire, localisation imprecision gives rise to substantial effects on the directionality and it is important to have this in mind as a control.

We start by looking at the directionality in terms of $\langle\cos\theta\rangle$ where brackets here denote average over time along a trajectory (Fig. 3a). We define the displacements for the shortest sampled time ($\Delta\tau$ equal to the time between frames; Fig. 2a) and study the directionality as a function of the separation in time between the displacements (as a function of τ). Fig. 3a shows the results for a few different particles, but the results are very similar particle-by-particle: naturally all curves start at $\langle\cos\theta\rangle = 1$, as a displacement is always in the same direction as itself. For successive displacements ($\tau = \Delta\tau$) $\langle\cos\theta\rangle$ shows a substantial negative value, meaning that the two displacements are in opposite directions. For displacements separated in time ($\tau > \Delta\tau$) $\langle\cos\theta\rangle$ is close to 0, meaning that there is no preferred direction.

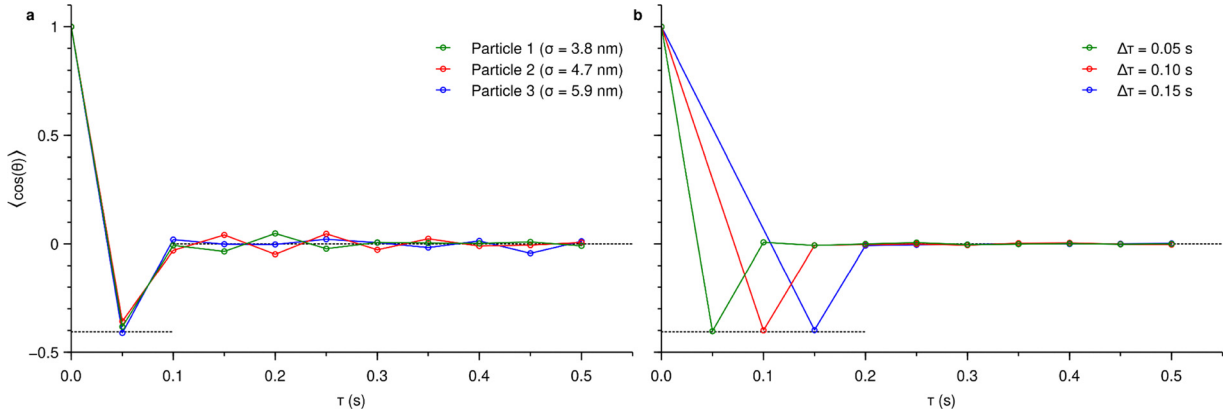

Fig. 3 Average $\cos\theta$ *vs.* time for stationary particles. Cosine of the angle θ between displacements as a function of the time τ separating the displacements averaged over time. See Fig. S2 for the equivalent results for the angle θ itself. (a) Displacements defined for the shortest sampled time ($\Delta\tau$ = 0.05 s, the time between frames; Fig. 2a). Successive displacements ($\tau = \Delta\tau$) thus correspond to τ = 0.05 s, while displacements separated in time from each other ($\tau > \Delta\tau$) correspond to τ = 0.10 s, 0.15 s *etc.* Results are shown for three different exemplar particles with different localisation imprecisions σ. (b) Different timescales $\Delta\tau$ used to define the displacements. $\Delta\tau$ = 0.05 s corresponds to the time between frames (as in panel a; Fig. 2a) while $\Delta\tau$ = 0.10 s corresponds to displacements defined over two frames (Fig. 2b) *etc.* The results have been averaged over all particles. (Dotted lines) Predicted values according to the theory developed below for successive displacements [$\langle\cos\theta\rangle \approx -0.406$; eqn (5) with $\rho = -\frac{1}{2}$] and displacements separated in time from each other [$\langle\cos\theta\rangle = 0$; eqn (5) with $\rho = 0$], respectively.

How do these results depend upon the timescale we used to define the displacements ($\Delta\tau$)? Given that the results are very similar for different particles, we average over particles and consider $\langle\cos\theta\rangle$ for different timescales $\Delta\tau$ (Fig. 3b). The results are qualitatively identical to when the displacements are defined for the shortest sampled time: $\langle\cos\theta\rangle$ starts at unity, then immediately becomes negative for successive displacements ($\tau = \Delta\tau$), and again immediately turns to 0 for displacements separated in time ($\tau > \Delta\tau$). The only difference is that the time at which $\langle\cos\theta\rangle$ becomes negative and 0, respectively, is different, but it is always the next successive displacement and the displacement after that. For even longer timescales used to define the displacements ($\Delta\tau$) we make the same observations (Fig. S1).

If we instead consider the mean of the angle θ itself rather than its cosine we make very similar observations (Fig. S2).

We now turn to the full distribution of the angle (Fig. 4 and Fig. S3), where we make analogous observations. For successive displacements ($\tau = \Delta\tau$), the distribution is highly skewed towards angles larger than $\pi/2$ (Fig. 4a), meaning displacements in the opposite direction. In contrast for displacements separated in time ($\tau > \Delta\tau$) the distribution is to a good approximation uniform (Fig. 4b). Again, we make the same observations (Fig. S4 and S5) for longer timescales used to define the displacements ($\Delta\tau$).

θ and $\cos\theta$ are unlikely to be directly dependent on the localisation imprecision σ as they are both dimensionless. In search of a quantity that more quantitatively can demonstrate

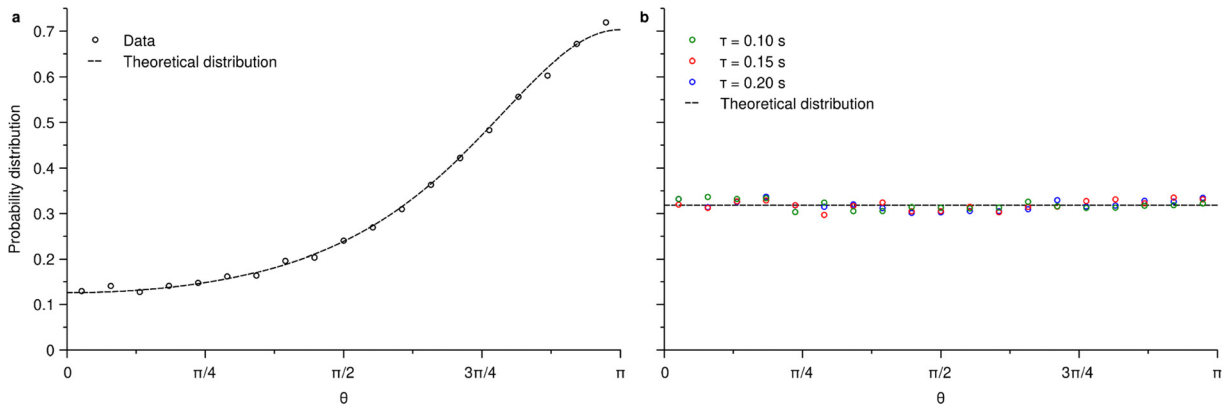

Fig. 4 Distribution of the angle between displacements for stationary particles. The displacements were defined for the shortest sampled time ($\Delta\tau$ = 0.05 s, the time between frames; Fig. 2a). Data from all particles have here been pooled together; the results for some exemplar individual particles are shown in Fig. S3. Angle θ between (a) successive displacements ($\tau = \Delta\tau$ = 0.05 s); and (b) displacements separated in time from each other ($\tau = 2\Delta\tau$ = 0.10 s, $3\Delta\tau$ = 0.15 s and $4\Delta\tau$ = 0.20 s). (Dashed lines) Predicted distributions according to the theory developed below for successive displacements [eqn (4) with $\rho = -\frac{1}{2}$; panel a] and displacements separated in time from each other [eqn (4) with $\rho = 0$; panel b].

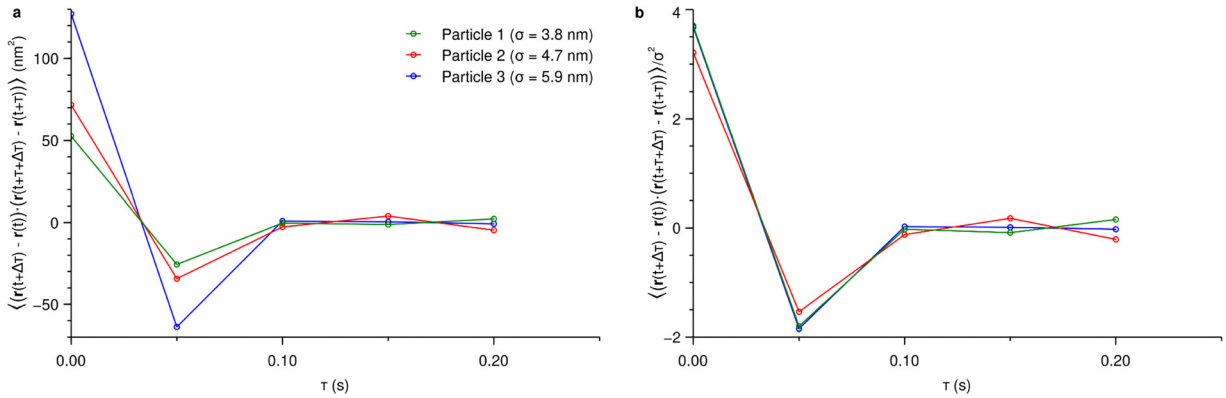

Fig. 5 Average scalar product [eqn (3)] *vs.* time for some exemplar stationary particles. Scalar product between displacements as a function of the time τ separating the displacements averaged over time. The displacements were defined for the shortest sampled time ($\Delta\tau$ = 0.05 s, the time between frames; Fig. 2a). Successive displacements ($\tau = \Delta\tau$) thus correspond to τ = 0.05 s, while displacements separated in time from each other ($\tau > \Delta\tau$) correspond to τ = 0.10 s, 0.15 s *etc.* Results are shown for three different exemplar particles with different localisation imprecisions σ. (a) Actual scalar product. (b) Scalar product normalised by the localisation imprecision squared σ^2.

the effect of a limited localisation imprecision, we thus consider the numerator of the right-hand side of eqn (1), that is, the scalar product

$$(\mathbf{r}(t+\Delta\tau)-\mathbf{r}(t))\cdot(\mathbf{r}(t+\tau+\Delta\tau)-\mathbf{r}(t+\tau)) \qquad (3)$$

which clearly has dimensions of area.

The mean of this quantity is closely related to the velocity autocorrelation function [*cf.* eqn (2)]. We thus start with the mean scalar product and follow how it changes as a function of the separation in time between the displacements (*i.e.*, as a function of τ; Fig. 5). The mean scalar product starts out positive ($\tau = 0$), then turns negative for successive displacements ($\tau = \Delta\tau$), and finally becomes close to 0 for displacements separated in time ($\tau > \Delta\tau$; Fig. 5a). The extent of the variation is strongly dependent on the localisation imprecision of the specific particle with particles with larger localisation imprecision showing a larger variation. In fact, if we rescale the curve by the localisation imprecision squared σ^2 then the data collapses onto a universal curve and we observe that the starting point is close to $4\sigma^2$ while the minimum is close to $-2\sigma^2$ (Fig. 5b).

Furthermore, we consider the distribution of the scalar product for a few different particles of different localisation imprecisions in Fig. 6a and b. For all particles we observe that the distribution is asymmetric for successive displacements ($\tau = \Delta\tau$; Fig. 6a) and symmetric for displacements separated in time ($\tau > \Delta\tau$; Fig. 6b). While the shape of the distribution is clearly the same for different particles, the extent of the distributions vary. Indeed, the larger the localisation imprecision, the more extended a distribution.

Since the only relevant length scale is the localisation imprecision, we expect the scalar product to be directly proportional to the localisation imprecision squared σ^2. This would clearly be consistent with the behaviour of the mean scalar product (Fig. 5b). Indeed, if we rescale the scalar products, the results to a good approximation fall upon a master curve (Fig. S6). We can consequently pool data from all particles together after such a rescaling (Fig. 6c and d).

Directionality of stationary particles – theoretical analysis

How can we understand these observations? It is possible to perform a detailed mathematical analysis. However, before doing so let us begin with an intuitive explanation of the general observation (Fig. 3–6 and Fig. S1–S6) that successive displacements are typically in opposite directions when observing stationary particles with finite localisation imprecision. Thus, consider a stationary particle fixed at some position. The first time the particle is imaged, it is observed not at its *actual* position (Fig. 7 real position) but at some other position since the particle cannot be localised with perfect precision. For the sake of argument say the observed position is shifted a substantial distance to the right (Fig. 7 observed position 1). Now consider the next time the particle is imaged. It will again be observed at a different position compared to its real position (Fig. 7 observed position 2). However, if the first position was shifted to the right from the original position then it is unlikely that the second position is shifted even more to the right; rather it is more likely that the second observed position is to the left of the first observed position (*cf.* Fig. 7 observed position 2 and 1). Of course, the first position might have been shifted slightly less to the right from the original position, and in that case it would have been somewhat less likely that the second position was to the left of the first position, but still rather likely *etc.* Overall, though, the vector connecting the real position with the first observed position and the vector connecting the first observed position with the second are more often than not in the opposite direction (Fig. 7 vectors).

A key ingredient of this argument is that the first observed position is included in both of the vectors we are comparing (the one connecting the real position to the first observed position, and the two observed positions). This introduces a correlation between the two different vectors, which is essential for the outcome that they are typically in opposite directions. If instead we were to consider two random vectors then they would naturally be pointing as often in the same direction as in the opposite.

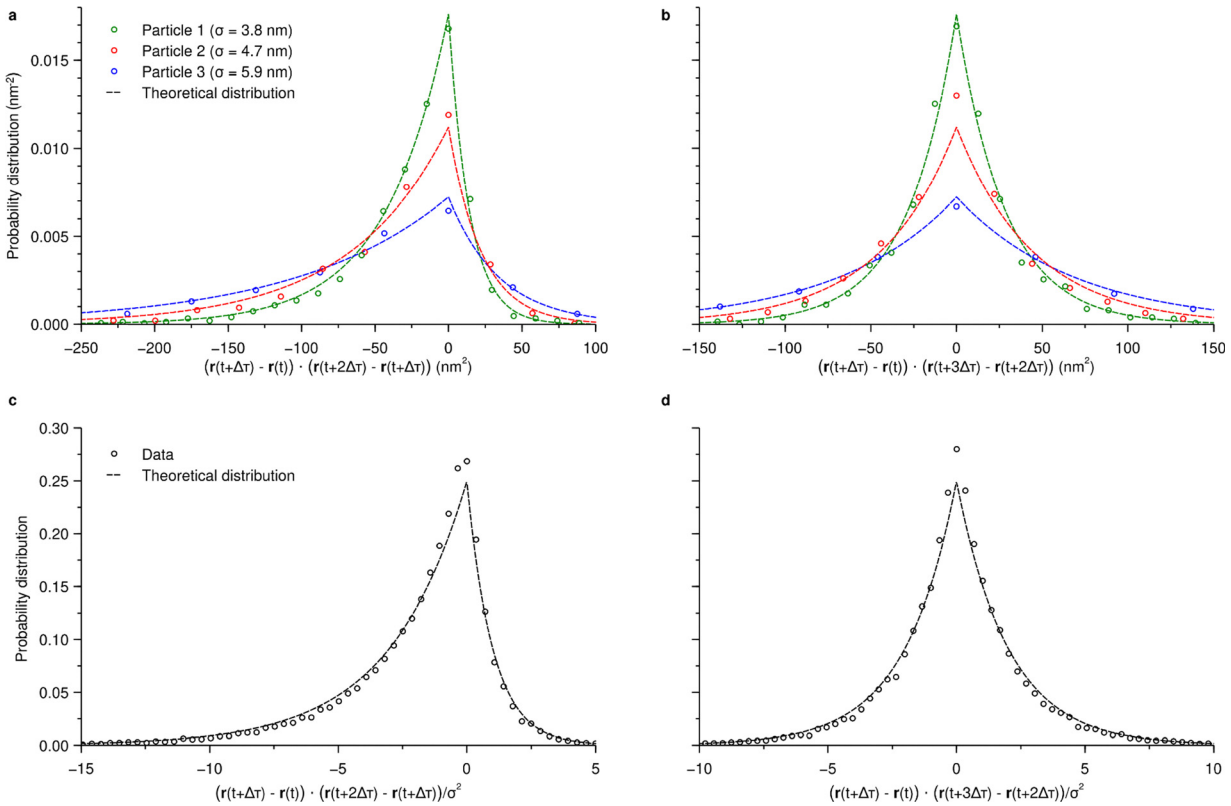

Fig. 6 Distribution of scalar product [eqn (3)] for stationary particles. The displacements were defined for the shortest sampled time ($\Delta\tau$ = 0.05 s, the time between frames; Fig. 2a). Scalar product between (a) and (c), successive displacements ($\tau = \Delta\tau$ = 0.05 s); and (b) and (d), displacements separated in time from each other ($\tau = 2\Delta\tau$ = 0.10 s). (a) and (b) Results for three different exemplar particles with different localisation imprecisions σ. (c) and (d) Data from all particles pooled together after the scalar product was normalised by the localisation imprecision squared σ^2 of each individual particle. (Dashed lines) Predicted distributions according to the theory developed below for successive displacements [eqn (7); panel a, c] and displacements separated in time from each other [eqn (8); panel b, d], respectively.

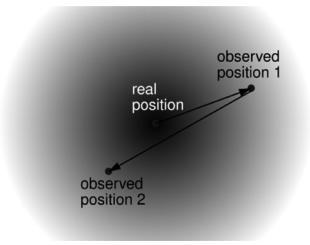

Fig. 7 Intuitive explanation for why successive displacements are typically in opposite directions for stationary particles observed with finite localisation imprecision. A particle has a certain location (real position) but there is a certain probability (greyscale) of it being observed at some distance away from its real position due to localisation imprecision. If a particle is observed multiple times (observed position 1 and 2) then it is likely that those observations will be in the opposite direction from each other.

These considerations thus argue for the direction typically being in the opposite direction when considering successive displacements, but the direction being completely random when considering displacements separated in time from each other. Indeed, this is what we observe experimentally (Fig. 3–6 and Fig. S1–S6). It should, however, be noted that to simplify the argument we have here phrased it in terms of the vector connecting the real position with the first observed position; the actual situation is that the real position is not known and hence the argument should be phrased in terms of the 3–4 positions needed to define two displacement vectors (Fig. 2). Our simplified argument nevertheless carries the heart of the matter, as the more detailed analysis indeed shows:

Thus, we consider a particle fixed at a certain position and imaged at various times. While the object remains fixed, its *observed* position fluctuates due to localisation imprecision. Consistent with experimental observations (Fig. 1c) we assume that the fluctuation in observed position at any of the investigated times is a normally distributed stochastic variable with mean 0 and a standard deviation equal to the localisation imprecision σ for the given particle. While we assume that the observed position at the different times share the same distribution, we furthermore assume that they are independent stochastic variables. There are situations where this is not necessarily true. For example, drift of the microscopy stage could lead to a correlation of the localisation imprecision at different observation times. It is clear that such correlations are not the source of the general observations we make in our experiments because by varying the timescale $\Delta\tau$ we use to define the displacement vectors we will also vary the magnitude

of any correlations. Doing so, however, does not affect the observations (Fig. S1 and S4, S5). There is a similar effect if the particles are actually moving: the microscopical observation always takes a finite amount of time, which means that the fluorescence emitted from the particle will spread out in the direction of movement and lead to a temporal correlation in the localisation imprecision. We will not take that into account here as we are only considering stationary particles but it has been discussed for Brownian motion in previous literature.[21,33]

Under the stated assumptions, it is possible to derive analytical formulae for all the results we have investigated experimentally. Some of these derivations are fairly lengthy so for brevity and readability we have relegated them to the SI (document titled "Explicit mathematical derivations") and only quote the outcomes here. While we are mainly interested in two dimensions, the SI also presents the results in one dimension for completeness.

We start with the distribution $f(\theta)$ of the angle between displacements θ: by passing to complex stochastic variables[41] and using a result from the signal processing literature,[42] one can show that it is given by [eqn (37) of the SI "Explicit mathematical derivations"]

$$f(\theta) = \frac{1}{\pi}\frac{1-\rho^2}{1-\rho^2\cos^2\theta}\left(1+\frac{\rho\cos\theta\arccos(-\rho\cos\theta)}{\sqrt{1-\rho^2\cos^2\theta}}\right) \quad (4)$$

ρ is here a parameter (the correlation coefficient between displacements; see SI "Explicit mathematical derivations" for its definition) which contains the whole time-dependence. Specifically, for successive displacements ($\tau = \Delta\tau$) we have $\rho = -\frac{1}{2}$, while for displacements separated in time from each other ($\tau > \Delta\tau$) we have $\rho = 0$. Thus, ρ is independent of the localisation imprecision. As a consequence the distribution of the angle is independent of the localisation imprecision as both expected and observed experimentally (Fig. S3). In more detail, for displacements separated in time from each other ($\tau > \Delta\tau$) $\rho = 0$ and the distribution simply reduces to $f(\theta) = 1/\pi$. This is perfectly in line with experimental observations (Fig. 4b and Fig. S4 and S5). Conversely, for successive displacements ($\tau = \Delta\tau$) $\rho = -\frac{1}{2}$ and we have a non-trivial and parameter-free prediction [eqn (4) inserting $\rho = -\frac{1}{2}$] for the shape of the distribution of the angle θ. This distribution has actually been derived previously in a completely different context (animal movement data investigated using GPS)[43] and our results are mathematically equivalent (as demonstrated by the derivation of eqn (38) in the SI "Explicit mathematical derivations"). In any case, this prediction from the theoretical analysis exhibits an excellent agreement with the experimental results (dashed line and data symbols in Fig. 4a; see also Fig. S3–S5).

From eqn (4) one can show that the average cosine of the angle between displacements is given by [eqn (39) of the SI "Explicit mathematical derivations"]

$$\langle\cos\theta\rangle = \frac{E(\rho)-(1-\rho^2)K(\rho)}{\rho} \quad (5)$$

where $K(\rho)$ and $E(\rho)$ are complete elliptic integrals of the first and second kind, respectively.[44] For successive displacements ($\tau = \Delta\tau$) $\rho = -\frac{1}{2}$ and we find $\langle\cos\theta\rangle \approx -0.406$. Conversely, for displacements separated in time from each other ($\tau > \Delta\tau$) $\rho = 0$ and the expression reduces to $\langle\cos\theta\rangle = 0$. Both of these results agree excellently with our experimental observations (dotted lines and data symbols in Fig. 3 and Fig. S1). Furthermore, the fact that we find different results for successive and displacements separated in time but otherwise no dependence on time also agrees perfectly with experiments (Fig. 3 and Fig. S1). The same goes for the independence on the localisation imprecision σ (Fig. 3a). We make the same observations for the mean angle (Fig. S2).

For the mean of the scalar product in eqn (3) one can readily show that [eqn (31) of the SI "Explicit mathematical derivations"]

$$\left\langle \big(\mathbf{r}(t+\Delta\tau)-\mathbf{r}(t)\big)\cdot\big(\mathbf{r}(t+\tau+\Delta\tau)-\mathbf{r}(t+\tau)\big)\right\rangle = \begin{cases} 4\sigma^2 & \tau = 0 \\ -2\sigma^2 & \tau = \Delta\tau \\ 0 & \tau > \Delta\tau \end{cases}. \quad (6)$$

This is again in excellent agreement with experimental observations (Fig. 5b). The mean of the scalar product is intimately related to velocity autocorrelation function [eqn (2)] and these results are also in agreement with previous theoretical results for the velocity autocorrelation function.[45]

Finally, using previously published results for the product of normally distributed variables[46,47] one can also calculate the distribution $f(s)$ of the scalar product eqn (3). For successive displacements ($\tau = \Delta\tau$) it is given by [eqn (28) of the SI "Explicit mathematical derivations"]

$$f(s) = \frac{1}{4\sigma^2}\begin{cases} e^{\frac{1}{3}s/\sigma^2} & s < 0 \\ e^{-s/\sigma^2} & s \geq 0 \end{cases}. \quad (7)$$

For displacements separated in time from each other ($\tau > \Delta\tau$) it is instead given by [eqn (29) of the SI "Explicit mathematical derivations"]

$$f(s) = \frac{1}{4\sigma^2}e^{-\frac{1}{2}|s|/\sigma^2}. \quad (8)$$

From these results we observe that the distribution is asymmetric for successive displacements and symmetric for displacements separated in time from each other. This is precisely as observed in the experiments (Fig. 6). Furthermore, for individual particles the theory gives an explicit prediction for the distribution and this prediction can be rendered parameter-free by taking the localisation imprecision σ from the experimental data. This prediction agrees very well with the experimental data (Fig. 6a and b).

Eqn (7) and (8) also show that the dependence on the localisation imprecision σ is simply what is expected based on dimensional analysis. Again this agrees with experiments (Fig. S6) and justifies our normalisation and pooling together of the results for different particles (Fig. 6c and d). Comparing the normalised data with the parameter-free prediction from theory also shows excellent agreement (Fig. 6c and d).

Overall we thus conclude that there is universal and excellent agreement between theory and experiments.

Directionality of particles moving by Brownian motion

Understanding the spurious directionality induced by localisation imprecision when observing stationary objects is of interest but obviously less interesting than objects that are actually moving. To challenge our understanding on moving objects, we therefore consider the archetypical example of stochastic motion – particles undergoing Brownian motion. Brownian motion exhibits no directionality of the motion so any directionality would be a curious observation. To demonstrate the effect, we expand upon the theoretical approach developed for stationary particles as theory allows easier variation of parameters compared to experiments. To check the theory we also perform simple simulations of Brownian motion (see Experimental section).

The complete mathematical derivation is again given in the SI (document titled "Explicit mathematical derivations"). Here we only quote the results we will actually use: for particles undergoing Brownian motion, the distribution of the angle between displacements and its average cosine are still given by eqn (4) and (5), respectively [and the mean angle between displacements by eqn (S1)]. It also remains true that $\rho = 0$ for displacements separated in time from each other [$\tau > \Delta\tau$; eqn (50) of the SI "Explicit mathematical derivations"]. This implies that we have no effect of localisation imprecision for displacements separated in time from each other ($\tau > \Delta\tau$). We will consequently focus our presentation on successive displacements ($\tau = \Delta\tau$). For successive displacements ($\tau = \Delta\tau$) the parameter ρ is now given by [eqn (48) of the SI "Explicit mathematical derivations"]

$$\rho = -\frac{1}{2}\frac{1}{1 + D\tau/\sigma^2} \tag{9}$$

where D is the particle diffusion coefficient.

Eqn (9) shows that the determining factor is the dimensionless quantity $D\tau/\sigma^2$. Intuitively we thus expect that when the diffusional length $\sqrt{(D\tau)}$ is much smaller than the localisation imprecision σ then localisation imprecision will dominate. Indeed, in the extreme scenario when $D = 0$, we regain the results for stationary particles. Conversely, when the diffusional length $\sqrt{(D\tau)}$ is much larger than the localisation imprecision σ we do not expect any effect of the localisation imprecision. Again, in the extreme scenario of $\sigma = 0$, we have $\rho = 0$ and no directionality is observed. Overall, we may view the localisation imprecision σ as a (fictitious) boundary; *within* this boundary we expect substantial effects of the localisation imprecision on the directionality while *beyond* this boundary we expect non-directional behaviour.

Fig. 8 shows the distribution $f(\theta)$ of the angle θ for a few different values of $D\tau/\sigma^2$. As expected, we observe that the distribution is identical to that for stationary particles when $D\tau/\sigma^2 = 0$ while there is no directionality when $D\tau/\sigma^2 = \infty$; the distribution varies between these two extremes for moderate values of $D\tau/\sigma^2$.

We next consider two fairly common experimental observables that quantify the mean directionality of the motion,

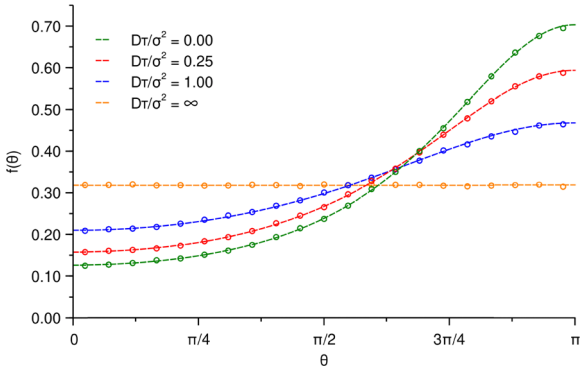

Fig. 8 Distribution of the angle between displacements for particles undergoing Brownian motion in the presence of localisation imprecision. Only successive displacements were considered. (Symbols) Results from simple numerical simulations varying the ratio of the diffusional length $\sqrt{(D\tau)}$ to the localisation imprecision σ. (Dashed lines) Predicted distributions according to theory [eqn (4) with ρ from eqn (9)].

namely the mean cosine of the angle (Fig. 9) or the mean angle (Fig. S7). We observe a strong effect of localisation imprecision for short times where $\langle\cos\theta\rangle$ tends to the limiting value expected for stationary particles (≈ -0.406). Conversely for longer times the effect of localisation imprecision vanishes and there is no directionality ($\langle\cos\theta\rangle = 0$). As expected the "transition" between localisation imprecision-dominated to diffusion-dominated behaviour occurs for $D\tau/\sigma^2 = 1$; however, note that there is a sizable average directionality even for $D\tau/\sigma^2$ as large as 10. While specifically for Brownian motion, we may use these results as a guide for setting up experiments. Thus, if we consider an average directionality of, say, $\langle\cos\theta\rangle > -0.05$ to be acceptable then the experiment should be set up such that $D\tau$ is greater than or equal to around $6.86\sigma^2$. Similarly, if it is only acceptable that $\langle\cos\theta\rangle > -0.01$, then one should take care to ensure that $D\tau$ is greater than or equal to around $38.3\sigma^2$.

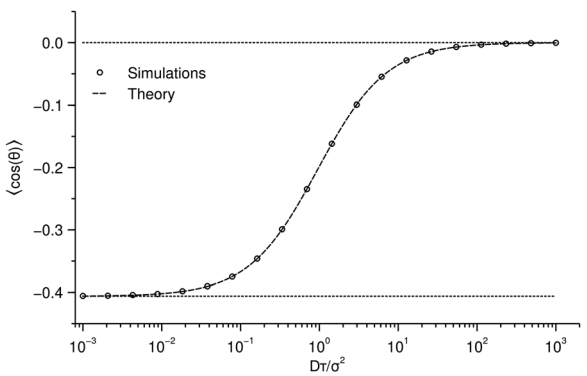

Fig. 9 Average $\cos\theta$ *vs.* time for particles undergoing Brownian motion in the presence of localisation imprecision. See Fig. S7 for the equivalent results for the angle θ itself. Only successive displacements were considered. Results are presented as a function of the ratio of the diffusional length $\sqrt{(D\tau)}$ to the localisation imprecision σ. (Symbols) Results from simple numerical simulations. (Dashed line) Prediction according to theory [eqn (5) with ρ from eqn (9)]. (Dotted lines) Limiting values: when $D\tau/\sigma^2 = 0$ we have $\langle\cos\theta\rangle \approx -0.406$ and when $D\tau/\sigma^2 = \infty$ we have $\langle\cos\theta\rangle = 0$. Note the log-scale.

It is reasonable to ask whether these effects are actually relevant experimentally. For the 200 nm particles used in this work we expect a diffusion coefficient in water at 20 °C of 2.14 $\mu m^2\ s^{-1}$ (using the Stokes–Einstein equation and a viscosity of water of 1001.6 μPa s).[48] Several of the figures discussed above (Fig. 3a, 5 and 6a, b, as well as Fig. S2 and S3 and S6) showed example results with a localisation imprecision around σ = 5 nm. With these values, the transition from localisation imprecision-dominated to diffusion-dominated occurs at a timescale of $\sigma^2/D \approx 12$ μs. This is quicker than most experimental set-ups. However, if we consider $D\tau/\sigma^2 = 8$ where there is still a noticeable effect of localisation imprecision (Fig. 9 and Fig. S7) then this occurs for a frame rate of $\approx 10^4$/s which is within range of modern microscopy cameras. Instead, consider 500 nm particles and a worse localisation imprecision of, say, σ = 25 nm. We then have a diffusion coefficient in water at 20 °C of 0.86 $\mu m^2\ s^{-1}$ and the transition occurs at a timescale of $\sigma^2/D \approx 0.91$ ms. This is undoubtedly within experimental limits.[28] Overall, we thus do not expect very large effects of the localisation imprecision on the directionality of particles moving by Brownian motion under typical conditions. However, the effect is certainly experimentally accessible. Furthermore, for slow-moving particles (large size or viscous medium) and/or large localisation imprecision the effects may even become substantial.

There are previous attempts at deriving the effect of localisation imprecision on particles undergoing Brownian motion. Thus, Weber *et al.* derived results that, under our assumptions and in our nomenclature, amounts to the mean scalar product in eqn (3). Their results read[45]

$$\langle(\mathbf{r}(t+\Delta\tau)-\mathbf{r}(t))\cdot(\mathbf{r}(t+\tau+\Delta\tau)-\mathbf{r}(t+\tau))\rangle = 4D\Delta\tau + 4\sigma^2$$

for $\tau = 0$, and

$$\langle(\mathbf{r}(t+\Delta\tau)-\mathbf{r}(t))\cdot(\mathbf{r}(t+\tau+\Delta\tau)-\mathbf{r}(t+\tau))\rangle = -2\sigma^2$$

for successive displacements ($\tau = \Delta\tau$), respectively. These results are exactly the same as our results [eqn (52) of the SI ''Explicit mathematical derivations'']. Furthermore, Harrison *et al.* also attempted to derive both the mean scalar product in eqn (3) as well as the average cosine of the angle between displacements in both cases for successive displacements.[28] However, they do not present results in terms of known parameters (such as the diffusion coefficient D and localisation imprecision σ) so we cannot directly compare.

Conclusions

As a general outcome we conclude that there is excellent and universal agreement between theory and experiments as well as between theory and simulations. This suggests that we have a good control and understanding of the role played by localisation imprecision in various measures of directionality when applied to stationary particles or particles moving by Brownian motion. Directionality quantification of stationary particles is in itself not interesting since they are not moving. The same goes for particles moving by Brownian motion since it is known that this type of motion is uniform. Our results are nevertheless useful as they provide a benchmark for just how large an effect localisation imprecision can have on directionality assessments and in particular demonstrate a considerable degree of anti-directionality.

Indeed, experimental studies in a range of different systems often report substantial anti-directional movements. For example, Raupach *et al.* followed the motion of micron-sized polystyrene beads on Mewo skin carcinoma cells.[25] The motion of the beads show a substantial degree of anti-directional movement at shorter times which reverts to mainly directional movement at longer times (their Fig. 7). Interestingly these authors did assess the directionality of stationary beads (their Fig. 7) and their results agree very well with ours (our Fig. 4a; see also Fig. S8 for a direct comparison to theory). Experiments on a related system of micron-sized ferrimagnetic beads on human airway smooth muscle cells show quite similar results.[26]

As another example, Munder *et al.* investigated the motion of self-assembled GFP-μNS particles in the yeast cytosol and report that it is anti-directional for short times.[15] They do argue that localisation imprecision is not the dominant source of the antidirectionality. Still, it is interesting to note that the average cosine of the angle they report for successive times (their Fig. 4 supplement 4) looks qualitatively similar to the above results (our Fig. 3). That is, $\langle\cos\theta\rangle$ starts at 1 (by definition) then becomes negative for successive displacements and tends to 0 for displacements separated in time. Quantitatively there is a difference though; the antidirectionality they report is only between around −0.1 to −0.3 depending upon condition whereas for stationary particles it is −0.406.

There are many other examples in the literature showing anti-directional movements[15,25,26,38,40,49,50] and while some studies do show the equivalent results under control conditions (*e.g.*, immobilised particles)[25,26] this is by no means a universal practice. We should stress that additional observations and arguments often support interpretations of anti-directional movement. Still, our results suggest that the *extent* of anti-directionality is likely overestimated if localisation imprecision is not properly accounted for.

In this context it is worth noting that a dip in the velocity autocorrelation function [eqn (2); in our nomenclature essentially the mean of the scalar product eqn (3)] is often used to interpret what type of motion occurs in a particular system.[8,51] Our results suggest that such a dip is expected even for stationary particles solely due to localisation imprecision. This was previously studied by Weber *et al.* in more detail.[45] However, we stress that localisation imprecision only gives such a dip for successive displacements whereas it is absent for displacements separated in time from each other (*cf.* Fig. 5). This is important because the velocity autocorrelation function is typically investigated as a function of the separation in time between the displacements (originally stemming from its definition as the correlation of *velocities*, not *displacements*). Thus, while the magnitude of the dip for successive displacements is affected by localisation imprecision, if the dip is there also for displacements separated in time from each other then the

presence of the dip itself is real. Thus, studies in the literature where such a dip is observed not just for the first investigated time (successive displacements) but also for subsequent times (displacements separated in time from each other) may be safely interpreted.[52–54]

The degree to which localisation imprecision affects assessments of directionality is even more complicated in systems which exhibit intermittent motion and this certainly includes many biological systems of interest.[55–57] In such systems we expect the directionality of the (at any given time) mobile particles to be appropriately quantified (assuming they move substantially longer than the localisation imprecision); in contrast we expect a substantial degree of anti-directional motion stemming solely from localisation imprecision from the immobile particles. Quantifying the directionality of the full ensemble of particles could then obscure the real directionality of the motion whether it is directional or uniform. In general we recommend caution when interpreting experimental quantifications of the directionality of motion stemming from microscopic observations.

Author contributions

P. M. M.: investigation, writing – original draft. C. Å.: conceptualization, supervision, investigation, writing – original draft.

Conflicts of interest

There are no conflicts to declare.

Data availability

The data supporting the conclusions drawn in this manuscript are contained within the article and supplementary information (SI). Supplementary information is available. See DOI: https://doi.org/10.1039/d6cp00367b.

Further inquiries may be directed to the corresponding author.

Acknowledgements

P. M. M. was supported by a Research Grant awarded to C. Å. from the Faculty of Science and Engineering, University of Groningen.

References

1 T. G. Mason, K. Ganesan, J. H. van Zanten, D. Wirtz and S. C. Kuo, *Phys. Rev. Lett.*, 1997, **79**, 3282–3285.
2 B. Stuhrmann, M. Soares e Silva, M. Depken, F. C. MacKintosh and G. H. Koenderink, *Phys. Rev. E: Stat., Nonlinear, Soft Matter Phys.*, 2012, **86**, 020901.
3 B. R. Parry, I. V. Surovtsev, M. T. Cabeen, C. S. O'Hern, E. R. Dufresne and C. Jacobs-Wagner, *Cell*, 2014, **156**, 183–194.
4 W. Feneberg, M. Westphal and E. Sackmann, *Eur. Biophys. J.*, 2001, **30**, 284–294.
5 M. Guo, A. J. Ehrlicher, M. H. Jensen, M. Renz, J. R. Moore, R. D. Goldman, J. Lippincott-Schwartz, F. C. Mackintosh and D. A. Weitz, *Cell*, 2014, **158**, 822–832.
6 H. Qian, M. P. Sheetz and E. L. Elson, *Biophys. J.*, 1991, **60**, 910–921.
7 H. Shen, L. J. Tauzin, R. Baiyasi, W. Wang, N. Moringo, B. Shuang and C. F. Landes, *Chem. Rev.*, 2017, **117**, 7331–7376.
8 R. Metzler, J.-H. Jeon, A. G. Cherstvy and E. Barkai, *Phys. Chem. Chem. Phys.*, 2014, **16**, 24128–24164.
9 B. Wang, S. M. Anthony, S. C. Bae and S. Granick, *Proc. Natl. Acad. Sci. U. S. A.*, 2009, **106**, 15160–15164.
10 J.-H. Jeon, V. Tejedor, S. Burov, E. Barkai, C. Selhuber-Unkel, K. Berg-Sørensen, L. Oddershede and R. Metzler, *Phys. Rev. Lett.*, 2011, **106**, 048103.
11 A. V. Weigel, B. Simon, M. M. Tamkun and D. Krapf, *Proc. Natl. Acad. Sci. U. S. A.*, 2011, **108**, 6438–6443.
12 S. M. A. Tabei, S. Burov, H. Y. Kim, A. Kuznetsov, T. Huynh, J. Jureller, L. H. Philipson, A. R. Dinner and N. F. Scherer, *Proc. Natl. Acad. Sci. U. S. A.*, 2013, **110**, 4911–4916.
13 F. Höfling and T. Franosch, *Rep. Prog. Phys.*, 2013, **76**, 046602.
14 N. Fakhri, A. D. Wessel, C. Willms, M. Pasquali, D. R. Klopfenstein, F. C. MacKintosh and C. F. Schmidt, *Science*, 2014, **344**, 1031–1035.
15 M. C. Munder, D. Midtvedt, T. Franzmann, E. Nüske, O. Otto, M. Herbig, E. Ulbricht, P. Müller, A. Taubenberger, S. Maharana, L. Malinovska, D. Richter, J. Guck, V. Zaburdaev and S. Alberti, *eLife*, 2016, **5**, e09347.
16 M. S. Song, H. C. Moon, J.-H. Jeon and H. Y. Park, *Nat. Commun.*, 2018, **9**, 344.
17 S. Thapa, N. Lukat, C. Selhuber-Unkel, A. G. Cherstvy and R. Metzler, *J. Chem. Phys.*, 2019, **150**, 144901.
18 E. Abbe, *J. R. Microsc. Soc.*, 1882, **2**, 300–309.
19 R. E. Thompson, D. R. Larson and W. W. Webb, *Biophys. J.*, 2002, **82**, 2775–2783.
20 L. Schermelleh, A. Ferrand, T. Huser, C. Eggeling, M. Sauer, O. Biehlmaier and G. P. C. Drummen, *Nat. Cell Biol.*, 2019, **21**, 72–84.
21 X. Michalet, *Phys. Rev. E: Stat., Nonlinear, Soft Matter Phys.*, 2010, **82**, 041914.
22 D. S. Martin, M. B. Forstner and J. A. Käs, *Biophys. J.*, 2002, **83**, 2109–2117.
23 X. Michalet and A. J. Berglund, *Phys. Rev. E: Stat., Nonlinear, Soft Matter Phys.*, 2012, **85**, 061916.
24 M. Weiss, *Phys. Rev. E*, 2019, **100**, 042125.
25 C. Raupach, D. P. Zitterbart, C. T. Mierke, C. Metzner, F. A. Müller and B. Fabry, *Phys. Rev. E: Stat., Nonlinear, Soft Matter Phys.*, 2007, **76**, 011918.
26 G. Lenormand, J. Chopin, P. Bursac, J. J. Fredberg and J. P. Butler, *Biochem. Biophys. Res. Commun.*, 2007, **360**, 797–801.
27 M. A. Despósito, C. Pallavicini, V. Levi and L. Bruno, *Phys. A*, 2011, **390**, 1026–1032.

28 A. W. Harrison, D. A. Kenwright, T. A. Waigh, P. G. Woodman and V. J. Allan, *Phys. Biol.*, 2013, **10**, 036002.
29 C. A. Schneider, W. S. Rasband and K. W. Eliceiri, *Nat. Methods*, 2012, **9**, 671–675.
30 J. Schindelin, I. Arganda-Carreras, E. Frise, V. Kaynig, M. Longair, T. Pietzsch, S. Preibisch, C. Rueden, S. Saalfeld, B. Schmid, J.-Y. Tinevez, D. J. White, V. Hartenstein, K. Eliceiri, P. Tomancak and A. Cardona, *Nat. Methods*, 2012, **9**, 676–682.
31 J.-Y. Tinevez, N. Perry, J. Schindelin, G. M. Hoopes, G. D. Reynolds, E. Laplantine, S. Y. Bednarek, S. L. Shorte and K. W. Eliceiri, *Methods*, 2017, **115**, 80–90.
32 P. Virtanen, R. Gommers, T. E. Oliphant, M. Haberland, T. Reddy, D. Cournapeau, E. Burovski, P. Peterson, W. Weckesser, J. Bright, S. J. van der Walt, M. Brett, J. Wilson, K. J. Millman, N. Mayorov, A. R. J. Nelson, E. Jones, R. Kern, E. Larson, C. J. Carey, İ. Polat, Y. Feng, E. W. Moore, J. VanderPlas, D. Laxalde, J. Perktold, R. Cimrman, I. Henriksen, E. A. Quintero, C. R. Harris, A. M. Archibald, A. H. Ribeiro, F. Pedregosa, P. van Mulbregt and SciPy 1.0 Contributors, *Nat. Methods*, 2020, **17**, 261–272.
33 T. Savin and P. S. Doyle, *Biophys. J.*, 2005, **88**, 623–638.
34 M. A. Thompson, J. M. Casolari, M. Badieirostami, P. O. Brown and W. E. Moerner, *Proc. Natl. Acad. Sci. U. S. A.*, 2010, **107**, 17864–17871.
35 P. Sil, N. Mateos, S. Nath, S. Buschow, C. Manzo, K. G. N. Suzuki, T. Fujiwara, A. Kusumi, M. F. Garcia-Parajo and S. Mayor, *Mol. Biol. Cell*, 2020, **31**, 561–579.
36 K. J. A. Martens, B. Turkowyd and U. Endesfelder, *Front. Bioinf.*, 2021, **1**, 817254.
37 S. Burov, S. M. A. Tabei, T. Huynh, M. P. Murrell, L. H. Philipson, S. A. Rice, M. L. Gardel, N. F. Scherer and A. R. Dinner, *Proc. Natl. Acad. Sci. U. S. A.*, 2013, **110**, 19689–19694.
38 W. Xu, E. Alizadeh and A. Prasad, *Biophys. J.*, 2018, **114**, 2933–2944.
39 M. Hu, H. Chen, H. Wang, S. Burov, E. Barkai and D. Wang, *ACS Nano*, 2023, **17**, 21708–21718.
40 M. Hidalgo-Soria, Y. Haddad, E. Barkai, Y. Garini and S. Burov, *arXiv*, 2024, preprint, arXiv:2407.08899, DOI: 10.48550/arXiv.2407.08899.
41 K. I. Park, *Fundamentals of probability and stochastic processes with applications to communications*, Springer International Publishing, Cham, 2018.
42 Y. Li, Q. He and R. S. Blum, *IEEE Signal Process. Lett.*, 2020, **27**, 16–20.
43 A. Hurford, *PLoS One*, 2009, **4**, e5632.
44 I. S. Gradshteyn and I. M. Ryzhik, *Table of integrals, series, and products*, Academic Press, 7th edn, 2014.
45 S. C. Weber, M. A. Thompson, W. E. Moerner, A. J. Spakowitz and J. A. Theriot, *Biophys. J.*, 2012, **102**, 2443–2450.
46 M. D. Springer, *The algebra of random variables*, Wiley, 1979.
47 L. P. Grishchuk, *Phys. Rev. D: Part. Fields*, 1996, **53**, 6784–6795.
48 W. M. Haynes, *CRC handbook of chemistry and physics: a ready-reference book of chemical and physical data*, CRC Press, Boca Raton, 91st edn, 2009.
49 N. Gal and D. Weihs, *Cell Biochem. Biophys.*, 2012, **63**, 199–209.
50 A. Mosqueira, P. A. Camino and F. J. Barrantes, *Sci. Rep.*, 2018, **8**, 11974.
51 R. Metzler and M. Weiss, *Phys. Chem. Chem. Phys.*, 2025, **27**, 14350–14358.
52 J. F. Reverey, J.-H. Jeon, H. Bao, M. Leippe, R. Metzler and C. Selhuber-Unkel, *Sci. Rep.*, 2015, **5**, 11690.
53 S. Stylianidou, T. J. Lampo, A. J. Spakowitz and P. A. Wiggins, *Phys. Rev. E*, 2018, **97**, 062410.
54 S. C. Weber, A. J. Spakowitz and J. A. Theriot, *Phys. Rev. Lett.*, 2010, **104**, 238102.
55 P. Bursac, G. Lenormand, B. Fabry, M. Oliver, D. A. Weitz, V. Viasnoff, J. P. Butler and J. J. Fredberg, *Nat. Mater.*, 2005, **4**, 557–561.
56 C. Åberg and B. Poolman, *Biophys. J.*, 2021, **120**, 2355–2366.
57 B. Corci, O. Hooiveld, A. M. Dolga and C. Åberg, *Soft Matter*, 2023, **19**, 2529–2538.

